Aerothermodynamic comparison of two- and three-dimensional rarefied hypersonic cavity flows

Journal of Spacecraft and Rockets (2014) Vol. 51, No. 5, pp. 1619-1630

Aerothermodynamic Comparison of Two- and Three-dimensional Rarefied Hypersonic Cavity Flows

Rodrigo C. Palharini*, Thomas J. Scanlon†,

James Weir Fluids Laboratory, University of Strathclyde, Glasgow G1 1XJ, United Kingdom

Jason M. Reese‡

School of Engineering, University of Edinburgh, Edinburgh EH9 3JL, United Kingdom

The thermal protection system is a key element in atmospheric reentry missions of aerospace vehicles. Usually, in the thermal load calculations, the analysis assumes that the vehicle has a smooth surface. However, discontinuities or imperfections are often present on the aerospace vehicle surfaces due to fabrication tolerances, sensor installations, spaces between the thermal protection plates, and differential expansion or ablation rates between non-similar materials. In the present work, rarefied hypersonic flows over two- and three-dimensional cavities at an altitude of 80 km in the Earth's atmosphere are studied numerically. In order to model flows in the transitional regime, where the validity of the Navier-Stokes equations is questionable, the direct simulation Monte Carlo method has been used. The primary goal is to assess the sensitivity of heat transfer, pressure, and skin friction coefficients for a family of two- and three-dimensional cavities defined by different length-to-depth ratios. The analysis shows that an assumption of two-dimensionality plays a key role in the over-prediction of the aerodynamic properties. Previous work using a continuum approach shows that two recirculation regions and flow attachment occurs when the length-to-depth ratio is greater than 14, however, the same phenomena are observed in the transitional regime when the cavity length-to-depth ratio is greater than 4. A study of the influence of the cavity width has also been conducted. It is shown that increasing the cavity width results in an augmentation of the surface aerothermodynamic quantities.

*PhD Candidate, Department of Mechanical and Aerospace Engineering.
†Senior Lecturer, Department of Mechanical and Aerospace Engineering.
‡Regius Professor of Engineering, School of Engineering.

Nomenclature

a	Speed of sound, m/s
C_f	Skin friction coefficient, Eq.(5)
C_h	Heat transfer coefficient, Eq.(1)
C_p	Pressure coefficient, Eq.(3)
c	Molecular velocity, m/s
D	Cavity depth, mm
d	Molecular diameter, m
H	Domain height, mm
Kn	Knudsen number, λ/L
L	Cavity length, mm
Ma	Mach number, U/a
m	Molecular mass, kg
n	Number density, m^{-3}
N	Number of particles
p	Pressure, $\mathrm{N/m}^2$
q	Heat flux, $\mathrm{W/m}^2$
R	Re-entry capsule nose radius, mm
Re	Reynolds number, UL/μ
T	Temperature, K
U	Freestream velocity, m/s
u, v	Normal and tangential velocity components, m/s
X'_L	Cavity length, dimensionless
X'_{L_d}	Downstream cavity length, dimensionless
X_{L_u}	Upstream cavity length, dimensionless
x, y, z	Cartesian axes in physical space, mm
Y_D	Cavity depth, dimensionless
W	Cavity width, mm
W_p	Plate width, mm
λ	Molecular mean free path, m
μ	Viscosity, $\mathrm{Ns/m}^2$
ρ	Density, $\mathrm{kg/m}^3$
τ	Shear stress, $\mathrm{N/m}^2$

ω Dynamic viscosity index, dimensionless

Subscripts

d Downstream surface

u Upstream surface

w Wall conditions

∞ Freestream conditions

I. Introduction

During the re-entry phase, aerospace vehicles are exposed to extreme thermal and aerodynamic loads requiring careful design of a heat shield. Generally, designers try to keep this surface smooth, but discontinuities between the thermal protection plates have to be expected due to sensor installation, fabrication tolerances, and differential expansion rates of non-similar materials. Such surface discontinuities may constitute a potential source of enhanced heat flux to the vehicle surface, or even cause a premature transition from laminar to turbulent flow.

In order to operate safely, these undesired thermal loads need to be correctly assessed.[1,2] This can be carried out either by using experiments, which are often very expensive for real flight conditions, or by numerical simulation, which is of continually increasing importance.[3–5] Several experimental, numerical, and theoretical studies have been conducted for the purpose of investigating the impact of imperfections present on the vehicle's surface on the aerodynamic properties.[6–21] For conciseness, only a selection of these studies will be discussed.

According to Charwat *et al.*,[6,7] flows over a cavities are typically classified as either open, closed, or transitional. In open cavity flows ($1 < L/D < 10$), the external flow passes over the cavity and the separated shear layer re-attaches near the top corner of the upstream-facing wall, thus producing recirculation inside the cavity. For closed cavity flows ($L/D \geq 14$), the separated shear layer re-attaches to the cavity floor upon followed by a further separation at the corner where the upstream face meets the freestream. The intermediary state between the two types, where the flow may also switch from one to the other, is termed as transitional ($10 < L/D < 14$).

Nestler *et al.*[11] conducted an experimental investigation on cavities and steps in hypersonic turbulent flow. For the flow conditions investigated, they found that the pressure distributions in the cavity exhibited the typical behavior of a closed cavity flow in the sense that the flow expands into the cavity, reattaches to the floor and separates at the downstream corner.

Everhart *et al.*[18] investigated experimentally the effect of a pressure gradient on the local heating distribution in rectangular cavities under hypersonic flow conditions. According to this experimental study,

the pressure gradient magnitude had an insignificant effect on the surface properties at the cavity shoulder. On the other hand, for long cavities, the pressure gradient magnitude played a significant role with the average surface heating rate increasing, in some instances, by a factor of 50% above the zero gradient conditions.

Unsteady hypersonic flows over annular cavities were investigated experimentally and numerically by Creighton and Hillier.[20] The objective of their study was to distinguish between weak and strong temporal oscillations due to different length-to-depth cavity ratios. According to the authors, a highly oscillatory motion exists which causes the movement of the separation point away from the forward lip and on to the fore-body of the cavity. They also highlighted the multi-dimensional nature of the flow structures created within the cavities.

The majority of studies in the literature have focused solely on a continuum-fluid approach to the laminar or turbulent aspects of hypersonic flow over cavities. It is apparent that, little work has been conducted on the physical aspects of rarefied hypersonic flow past three-dimensional cavities in a re-entry environment.

The present paper extends the previous analysis of Palharini and Santos[21] by investigating the three-dimensional impact on the cavities' aerodynamic surface quantities. The primary goal is to assess the sensitivity of heat transfer, pressure, and skin friction coefficients for a family of 2D/3D cavities defined by different length-to-depth ratios (L/D).

At high altitudes, the collisional time and length scales are large in comparison to those associated with the flow geometry and macroscopic variable gradients, and individual particles experience few collisions over the macroscopic time scales.[22,23] In such conditions, the molecular velocity distribution can diverge significantly from the equilibrium distribution and the continuum governing equations tend to break down. Thus, conventional computational fluid dynamics (CFD), using the Navier-Stokes-Fourier equations, becomes inappropriate. A particle-based approach is necessary and the direct simulation Monte Carlo (DSMC) technique has therefore been employed in the present account for solving flows over 2D/3D cavities.

This paper is organized into six further sections. In Section II, the cavity geometric parameters are defined. Section III deals with the computational procedures employed and includes details about the DSMC methodology adopted. The boundary conditions and analysis procedure are discussed in Section IV, while Section V presents the freestream gas properties for the selected altitude of 80 km. In Section VI, results are presented that describe the major flow features and surface aerothermodynamic properties for both 2D and 3D cavities, including the effect of cavity width. Finally, Section VII presents conclusions and recommendations for future work.

II. Geometry Definition

Discontinuities or imperfections on the vehicle's surface have been modeled as two- and three-dimensional cavities defined by a length L and a depth D. By considering that the depth D is much smaller than the nose radius R of the reentry vehicle, i.e., $D/R \ll 1$, then the environmental conditions may be represented by hypersonic flow over a flat plate with a cavity, as shown in Figure 1.

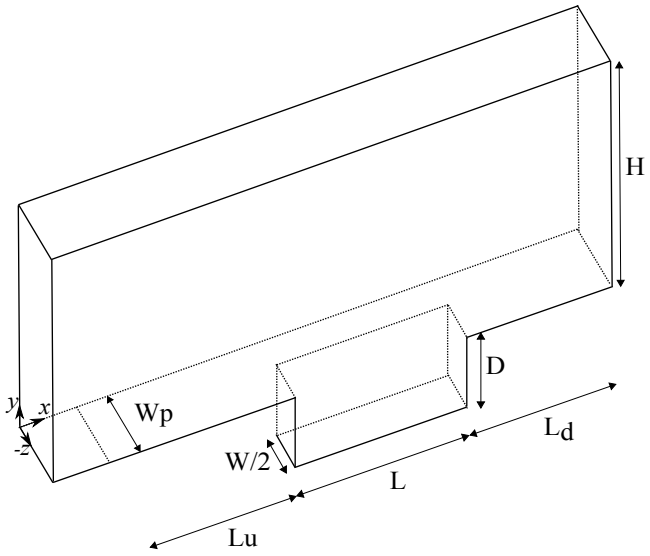

Parameter	2 D cases (mm)	3 D cases (mm)
Length (L)	3, 6, 9, 12	3, 6, 9, 12
Depth (D)	3	3
Width (W/2)	–	1.5, 3.0
Height (H)	30	30
Plate width (W_p)	–	12
Upstream length (L_u)	50	50
Downsteam length (L_d)	50	50

Figure 1. Schematic of the cavity configuration and its main geometrical parameters.

III. Computational Method and Procedure

The most successful numerical technique for computing rarefied hypersonic flows is the direct simulation Monte Carlo (DSMC) method, pioneered by Bird.[24] Based on Bird's algorithm, new freeware called *dsmcFoam* has been developed to solve complex engineering problems appropriate for rarefied gas conditions.[25] This new DSMC solver has been developed within the framework of the open-source computational fluid dynamics toolbox OpenFOAM.[26] The main features of the *dsmcFoam* code include particle initialization in arbitrary geometries, particle tracking in unstructured meshes, the capability to perform both steady state and transient DSMC simulations, and unlimited parallel processing.

The DSMC technique instructs particles to move and collide using kinetic-theory considerations that can capture the non-equilibrium gas behavior accurately. DSMC considers molecular collisions using stochastic rather than deterministic procedures over a time step which is a small fraction of the mean collision time, and each DSMC particle represents a large number of real gas molecules. The decoupling of particle ballistic motion and particle collisions improves the computational efficiency of DSMC greatly in comparison with

other particle methods such as molecular dynamics (MD). The computational domain is divided into either a structured or unstructured grid of cells, with each cell of a dimension that is a small fraction of the local mean free path. The cells are then utilised to select particles for collisions on a probabilistic basis, and also are used for sampling the macroscopic flow properties. Intermolecular collisions are handled probabilistically using phenomenological models that are designed to reproduce real fluid behavior when the flow is examined at the macroscopic level. The DSMC technique has been shown to provide a solution to the Boltzmann equation as the number of simulated particles tends toward infinity.[27]

In the present work, internal energy exchange is modeled using the Larsen-Borgnakke scheme,[28] the molecular collision kinetics are modeled using the variable hard sphere (VHS) molecular model,[24] and the no time counter (NTC) collision sampling technique.[29] Simulations are performed for a non-reacting rarefied hypersonic flow, consisting of 76.3% N_2 and 23.7% O_2, which represents the freestream conditions at an altitude of 80 km.

IV. Computational Domain and Grid

In order to implement the particle-particle collisions, the flowfield around the cavity is divided into a number of regions, which are subdivided into computational cells. The cells are further subdivided into subcells with two subcells per cell in each coordinate direction. The cell provides a convenient reference for the sampling of the macroscopic gas properties, while the collision partners are selected from the same subcell for the establishment of the collision rate; subcells promote nearest-neighbor collisions and therefore a more realistic transport of mass, momentum, and energy. The computational domain used for the calculation is made large enough such that cavity disturbances do not reach the upstream and side boundaries, where freestream conditions are specified. A schematic view of the computational domain is depicted in Fig. 2. The computational domain is divided into four regions, with side I-A defining the cavity surface, with diffuse reflection and complete momentum/thermal accommodation applied as a boundary condition. Side I-B is a symmetry plane, where all flow gradients normal to the plane are zero; at the molecular level, this plane is equivalent to a specular reflecting boundary. This boundary condition is also applied on the half-symmetry plane which bisects the 3D cavity. Sides II, III, and IV are defined as freestream, and simulated particles enter and exit the domain at these locations.

In the DSMC algorithm, the dimensions of the cells should be small in comparison with the length scale of the macroscopic flow gradients, which means that the cell dimensions should be of the order of (or even smaller than) the local mean free path.[30] The cell size also needs to be small enough to restrict collisions to nearby particles, but should, at the same time, contain a sufficient number of particles to maintain the statistical accuracy of the method. The time step should also be chosen to be sufficiently small in comparison

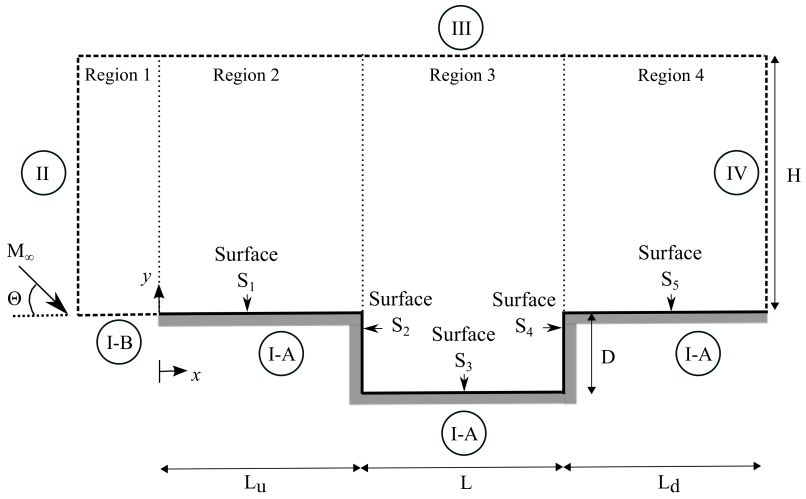

Figure 2. Schematic of the 2D computational domain.

with the local mean collision time.[4,31,32] In the present work, the time step and the mean collision time are 3.8×10^{-9} s and 1.1×10^{-5} s, respectively.

A grid independence study was executed with three different structured meshes (coarse, standard, and fine) for the largest 3D cavity and the results are presented in Fig. 3. The effect of altering the cell size in the x-direction was investigated for the coarse and fine grids with, respectively, 50% fewer and 50% more cells compared to the standard grid in the x-direction. In this way, the coarse, standard and fine grids corresponded to 429,300, 854,400 and 1,891,920 cells, respectively. Similarly, an investigation was made using a coarse and fine grid in the y-direction with, respectively, 50% fewer and 50% more cells compared to the standard grid in the y-direction.

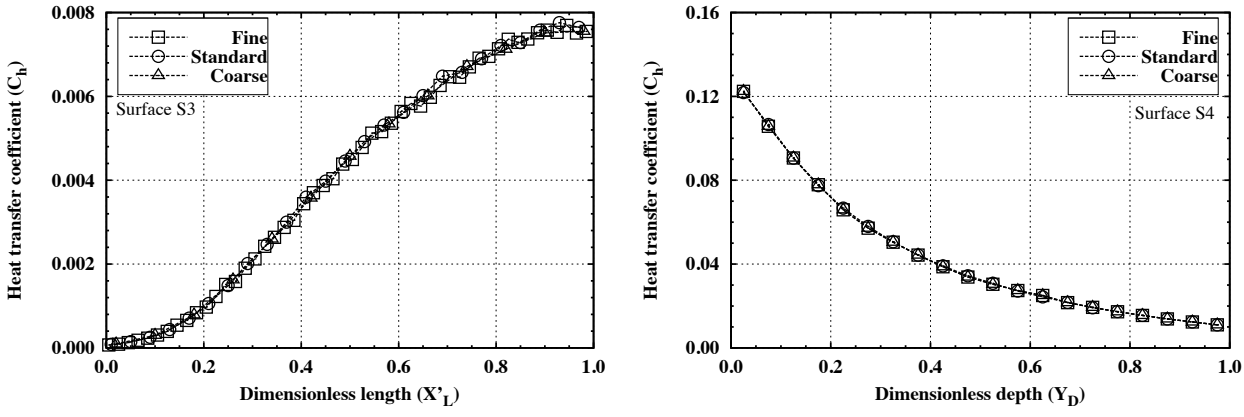

Figure 3. Influence of cell number on the heat transfer coefficient (C_h) for surfaces S_3 and S_4.

The effect of changing the cell size in both directions on the heat transfer, pressure and the skin friction coefficients was found to be rather insensitive for the range of cell spacings considered, indicating that the standard grid solution, with a total of 854,400 cells, for the $L/D = 4$ case, is essentially grid independent.

In a second stage of the grid independence investigation, a similar examination was made for the number of DSMC particles. The standard grid for the $L/D = 4$ case corresponds to, on average, a total of 8,600,000 DSMC particles. Two new cases using the standard grid were investigated. These corresponded to 4,300,000 and 17,000,000 particles in the full computational domain. As the three cases demonstrated approximately the same results for the heat transfer, pressure and skin friction coefficients, the standard grid with a total of 8,600,000 particles was considered sufficient for the computation of the relevant flowfield properties.

V. Freestream Conditions

The freestream conditions employed in the present calculations are shown in Table 1. These flow conditions represent those typically experienced by a capsule at an altitude of 80 km in the Earth's atmosphere.[33] The freestream velocity U_∞ is assumed to be constant at 7565.7 m/s, which corresponds to a freestream Mach number M_∞ of 25. The surface temperature T_w is assumed constant at 1000 K, which is chosen to be representative of the surface temperature near the stagnation point of a re-entry vehicle, and is assumed to be uniform over all surfaces including the cavity. It is important to highlight that the surface temperature is low compared to the stagnation temperature of the air. This assumption is reasonable since practical surface materials would be likely to disintegrate if the surface temperature approached the flow stagnation temperature.

Parameter	Value	Unit
U_∞	7565.7	m/s
T_∞	198.62	K
p_∞	1.05	N/m^2
ρ_∞	1.844×10^{-5}	kg/m^3
μ_∞	1.321×10^{-5}	Ns/m^2
n_∞	3.831×10^{20}	m^{-3}
λ_∞	3.850×10^{-3}	m

Table 1. Freestream flow conditions at 80 km altitude.

By assuming the cavity length L as the characteristic length, the Knudsen numbers Kn_L are 1.286, 0.643, 0.429, and 0.322 for cavity lengths of 3, 6, 9, and 12 mm, respectively. Finally, the Reynolds numbers Re_L are 31.68, 63.36, 95.04, and 126.73 for cavity lengths of 3, 6, 9, and 12 mm, respectively, based on conditions in the undisturbed freestream.

VI. Computational Results and Discussion

In the design of planetary re-entry vehicles, the primary variables to be analyzed are: heat transfer, pressure, and skin friction. These variables not only govern the aerodynamic performance of the vehicle body, but they are of particular importance for the design integrity of its heat shield. The purpose of this section is to present and discuss the behavior of these quantities, expressed in dimensionless form, for 2D/3D cavities of different length-to-depth ratios.

Before proceeding with the analysis of the aerodynamic surface quantities, it is instructive to present graphically the flow topology inside the cavities. Density ratio ρ/ρ_∞ contours with streamline traces inside the 2D and 3D cavities are shown in Fig. 4 for L/D ratios of 1, 2, 3 and 4. It is evident that the flow inside cavities is characterised by the recirculation structure. The streamline patterns for L/D ratios of 1 and 2 for 2D/3D simulations show that the flow has a primary vortex system, and the recirculating structure fills the entire cavity. For the $L/D = 3$ and 4 cases, a different flow structure is observed: two vortices are formed, one of them close to the upstream face and the other one in the vicinity of the downstream face of the cavity. The separated shear layer from the external stream does not reattach to the cavity floor, and the flow is reversed along the bottom cavity surface. Furthermore, for the $L/D = 4$ and 2D case, the recirculation regions are well defined and separated shear layer is able to penetrate deeper into the cavity and attach itself to the cavity base wall, enhancing momentum and energy transfer to the bottom surface. However, this behavior is not observed for the same configuration in a three-dimensional cavity.

It is important to highlight that in the continuum regime,[18] there are two recirculation regions and the flow impinges directly on the cavity floor when $L/D > 14$. The same phenomena is observed in the transitional regime when the cavity length-to-depth ratio is 4, or greater. Therefore, even a small cavity under rarefied gas conditions could promote serious damage to the heat shield during reentry. These results are more evident in Figs. 5, 6, and 7, and they are described in the following sections.

A. Heat Transfer Coefficient

The heat transfer coefficient C_h is defined as:

$$C_h = \frac{q_w}{\frac{1}{2}\rho_\infty U_\infty^3} \tag{1}$$

where the heat flux q_w to the body surface is calculated as the net energy flux of molecules impinging on the surface. A flux is regarded as positive if it is directed toward the body surface. The net heat flux q_w is related to the sum of the translational, rotational and vibrational energies of both incident and reflected

particles as defined by,

$$q_w = q_i - q_r = \frac{F_N}{A\Delta t}\sum_{j=1}^{N}\left\{\left[\frac{1}{2}m_j c_j^2 + e_{Rj} + e_{Vj}\right]_i - \sum_{j=1}^{N}\left[\frac{1}{2}m_j c_j^2 + e_{Rj} + e_{Vj}\right]_r\right\} \tag{2}$$

where F_N is the number of real molecules represented by a single simulated particle, Δt is the time step, A the cell surface area, N is the number of particles colliding with the surface per unit time and unit area, m is the mass of the particles, c is the velocity of the particles, and e_R and e_V are the rotational and vibrational energies, respectively. Subscripts i and r refer to incident and reflected particles.

The effect on the heat transfer coefficient C_h due to variation in the L/D ratio for 2D and 3D cases along the cavity center line is shown in Fig. 5 for surfaces S_1 to S_5. Here, X_{L_u}, X'_L, and X'_{L_d} represent the horizontal surface dimensions normalised by their respective lengths, and Y_D refers to the depth y normalised by the cavity depth D.

According to these plots, there are no apparent differences between the 2D and 3D results for the heat transfer coefficient along the surface S_1 from the leading edge up to the region around the upstream corner of the cavities. For the range of L/D ratios investigated, C_h is low at the leading edge, increases to a peak value of $C_h = 0.028$ at section X = 8.0, and then slightly decreases downstream towards the cavity upstream corner, i.e., at the junction of surfaces S_1 and S_2. Along the surface S_5, it is observed that C_h is largest at the leading edge of this surface and decreases downstream along the surface S_5 to a minimum value at the trailing edge.

For the backward facing, surface S_2, the heat transfer coefficient C_h is high at the cavity entrance $Y_D = 0$, and decreases to a minimum value close to the cavity corner. Along the cavity floor, surface S_3, C_h depends upon the L/D ratio and consequently on the flow structure inside the cavity. In general, C_h increases from near zero at location $X'_L = 0$ to reach a maximum at location $X'_L = 0.9$. In addition, the larger the L/D ratio the larger the maximum value attained by C_h. For the forward facing surface S_4, C_h is highest at the top of the cavity, and it is observed to decrease along the surface, reaching lower values at the junction of the surfaces S_3 and S_4.

It is evident that the inclusion of the third-dimension plays a key role in the magnitude of the surface properties and the general flow dynamics. In a full 3D simulation all of the cavity surfaces are included in an explicit manner and, consequently, the particles have a larger contact area to collide, thus enhancing the momentum and energy transfer. This extra area acts as an energy sink helping to reduce the overall energy budget of the particles. In addition, decreasing the particles' energy contributes to slower flow within the cavity and a consequent increase in particle residence time within the recirculating zone. This also makes it more difficult for freestream particles to penetrate deeper into the cavity.

B. Pressure Coefficient

The pressure coefficient C_p is defined as:

$$C_p = \frac{p_w - p_\infty}{\frac{1}{2}\rho_\infty U_\infty^2} \tag{3}$$

where the pressure p_w on the body surface is calculated as the sum of the normal momentum fluxes of both incident and reflected molecules at each time step, i.e.:

$$p_w = p_i - p_r = \frac{F_N}{A\Delta t}\sum_{j=1}^{N}\{[(mc_n)_j]_i - [(mc_n)_j]_r\} \tag{4}$$

where c_n is the normal component of the velocity of the DSMC particle j.

The variation of the pressure coefficient C_p along the cavity surfaces S_1 to S_5 is plotted in Fig. 6 for various L/D ratios. Along surface S_1 it is clear that C_p shows a similar behavior for all 2D and 3D cavities studied. However, along the surface S_5 it is observed that the L/D ratio plays an important role in the pressure augmentation at the leading edge of this surface. The presence of small discontinuities in the thermal protection system is almost imperceptible for the incoming freestream particles. However, by increasing the cavity length-to-depth ratio, the freestream is effectively disturbed by the presence of the cavity.

The pressure coefficient on surface S_2 is small at the cavity entrance, $Y_D = 0$, due the expansion around the upstream lip, but increases along the surface reaching a maximum value at location $Y_D = 0.6$ and then decreases towards the cavity corner. Along the cavity floor, surface S_3, C_p increases and reaches its maximum value near the junction of the surfaces S_3 and S_4. According to Fig. 4, a high density region is observed at this junction, which contributes to high pressure augmentation in this region.

Finally, along the forward facing, surface S_4, the pressure coefficient behavior contrasts with that observed along S_2, in the sense that C_p has its lowest value at the location $Y_D = 1.0$, and increases steadily along the surface, reaching a peak value at the shoulder (junction of S_4 and S_5), $Y_D = 0$. This is expected because the flow develops into a high compression region at this surface, mainly towards the cavity lip represented by the junction of the surfaces S_4 and S_5. It is important to highlight that the pressure coefficient at surface S_4 is an order of magnitude greater than at surfaces S_2 and S_3.

According to Fig. 4 and Palharini and Santos,[21] the streamline pattern for 2D cavities shows that the flow is characterised by a primary vortex system for $L/D = 1$ and 2, where a clockwise recirculation structure fills the entire cavity void. In contrast, for $L/D = 3$ and 4, the flow is characterised by two vortex systems in the vicinity of the backward and forward surfaces, with the freestream flow attaching to the cavity floor,

surface S_3. In addition, for 3D simulations and $L/D = 4$, the vortices remain connected whereas they are completely separate in the 2D case. In the 3D cavity configuration, the main flow is not able to attach to the bottom of the cavity, causing a decrease in the pressure load when compared with the 2D cases.

C. Skin Friction Coefficient

The skin friction coefficient C_f is defined as:

$$C_f = \frac{\tau_w}{\frac{1}{2}\rho_\infty U_\infty^2} \tag{5}$$

where the shear stress τ_w on the body surface is calculated as the sum of the tangential momentum fluxes of both incident and reflected molecules impinging on the surface at each time step,

$$\tau_w = \tau_i - \tau_r = \frac{F_N}{A\Delta t}\sum_{j=1}^{N}\{[(mc_t)_j]_i - [(mc_t)_j]_r\} \tag{6}$$

where c_t is the tangential velocity component of the velocity of the DSMC particle j.

For the special case of completely diffuse reflection, which is the gas-surface interaction model adopted in the present work, the reflected particles have a mean tangential momentum of zero, since the particles lose, on average, their tangential velocity components. The net tangential momentum flux therefore can be simplified to:

$$\tau_w = \tau_i = \frac{1}{A\Delta t}\sum_{j=1}^{N}[(mc_t)_j]_i \tag{7}$$

The impact on the skin friction coefficient C_f due to changes on the 2D/3D cavity L/D ratio is shown in Fig. 7, for surfaces S_1 to S_5. The skin friction coefficient for surfaces S_1 and S_5 follows a similar behavior to that described for the heat transfer coefficient C_h in Fig. 5. However, it is observed that the peak values for C_f along surfaces S_1 and S_5 are 66.7% and 69% larger, respectively, than those observed for the pressure coefficient. As a result, the tangential forces, associated with the shear stress, are larger than the normal forces, which are related to the wall pressure, in this region.

The skin friction coefficient along surface S_2 is highest at the cavity entrance, $Y_D = 0$, and decreases along this surface reaching a smaller value at the cavity corner. For the cavity floor, surface S_3, the C_f behavior is influenced by the value of L/D. It is negative in the vicinity of the S_2/S_3 junction, then it becomes positive and reaches a maximum value that depends on the L/D ratio. In contrast with surface S_2, on the forward

facing surface S_4 the skin friction coefficient is always negative.

Normally, when C_f changes from positive to negative, the condition $C_f = 0$ may indicate the presence of a backflow, an attachment or a reattachment point. Here, these are directly related to the clockwise recirculation structure, defined by a primary vortex system observed for the $L/D = 1$ and 2 cases, and two recirculating structures observed for the $L/D = 3$ and 4 cases.

D. Effect of cavity width

This section considers the influence of the cavity width on the predicted aerothermodynamic surface quantities. In order to highlight the essential features of this effect, we consider the normalised density contour plots and streamline traces inside the cavity, as shown in Fig 8.

It is evident that doubling the cavity width from 1.5 to 3.0 mm results in no appreciable change in the cavity flow structure for the length-to-depth ratios L/D = 1, 2 and 3. However, for $L/D = 4$, the flow structure inside the cavity resembles that found in the 2D cavity study with flow penetration being enhanced; streamline attachment to the cavity base is evident and two separate vortical regions are formed. It is also clear that the increased entrainment allows more particles to impact on the vertical cavity surface S_4 and, as a consequence, the dimensionless density on this surface reaches a maximum value of 5.5 while a maximum of 4.5 occurs for the 1.5 mm width case.

Figures 9, 10, and 11 show the effect of the cavity width on the surface aerothermodynamic properties along the center-line. It is evident that there is an insignificant change in the heat transfer, pressure and skin friction along surfaces S_1 and S_5. However, for the cavity internal surfaces, the increase in the cavity width does influence significantly the surface properties. The maximum difference of C_h, C_p and C_f was found to be 68%, 21.5% and 64%, respectively at the cavity floor for $L/D = 4$. This augmentation of the surface properties is directly related to the enhanced entrainment into the cavity as the width is increased, resulting in a larger number of particle surface impacts with the consequent increase in energy and momentum exchange with surfaces S_2, S_3, and S_4. It is clear that the cavity width can play an important role in the categorization of flows over surface discontinuities such as cavities, and further studies are necessary to fully comprehend the influence of this parameter.

VII. Conclusions

Computations of rarefied hypersonic flow over 2D and 3D cavities have been performed using the DSMC method. The calculations provide in-depth information concerning the nature of the aerothermodynamic surface quantities for a family different cavities. Effects of the length-to-depth ratio and three-dimensionality on the heat transfer, pressure, and skin-friction coefficients have been investigated. It was found, for the

range of conditions considered, that the flow structures differ markedly from those observed in the continuum regime. The addition of the third spatial dimension to the problem significantly alters the flow field in and around the cavities. The application of a 2D cavity solution will significantly over predict aerothermodynamic loads, with these being several times larger than those observed for a 3D study. Further investigations are suggested to fully categorize the influence of cavity width on the flow physics, with additional parameters such as Mach number, altitude, angle of attack, cavity shape, gas-surface interaction, and reacting flows considered as important areas of study.

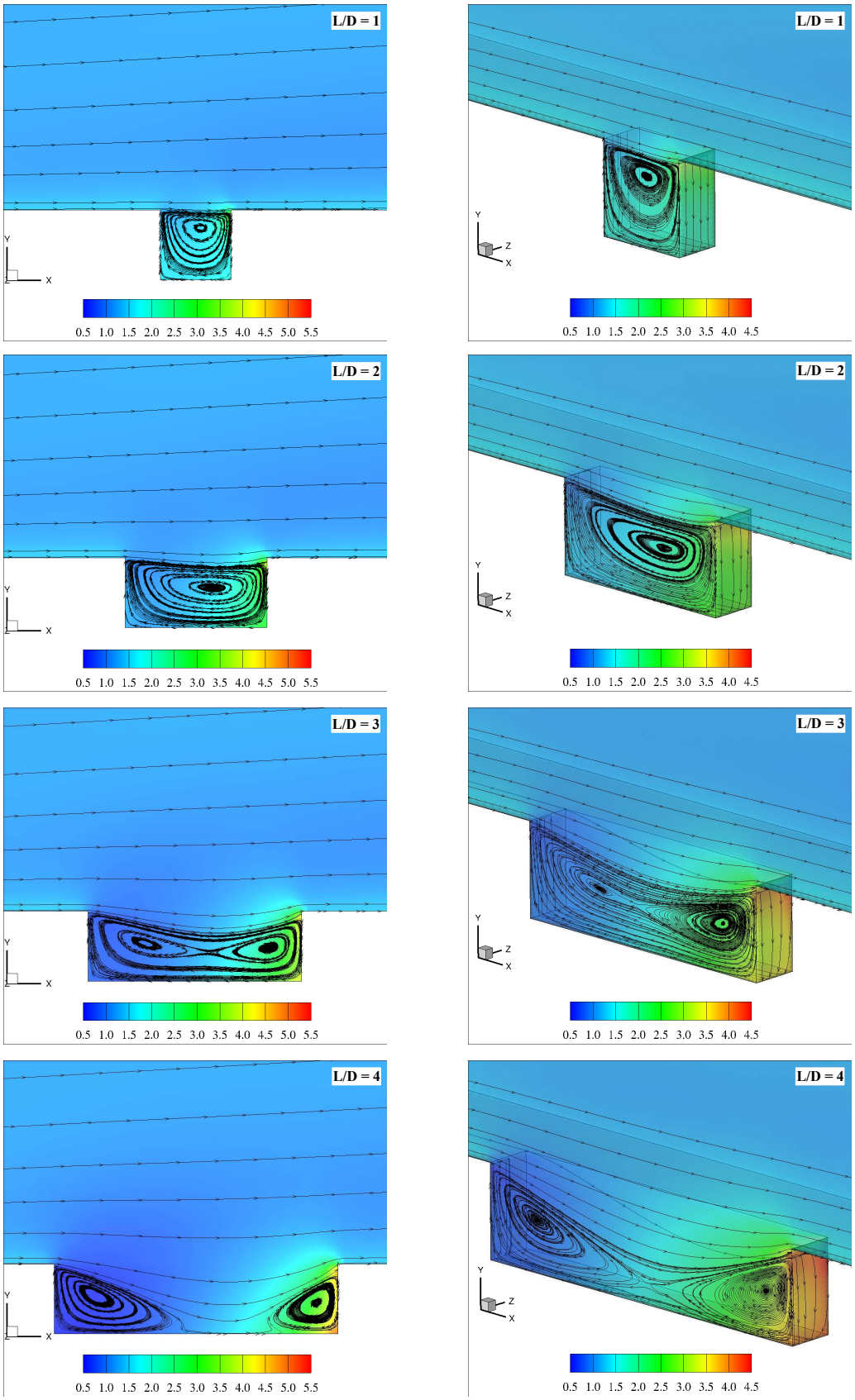

Figure 4. Density ratio (ρ/ρ_∞) contours, with streamline traces inside the cavities. Left: 2D cases, Right: 3D cases (W/2 = 1.5 mm).

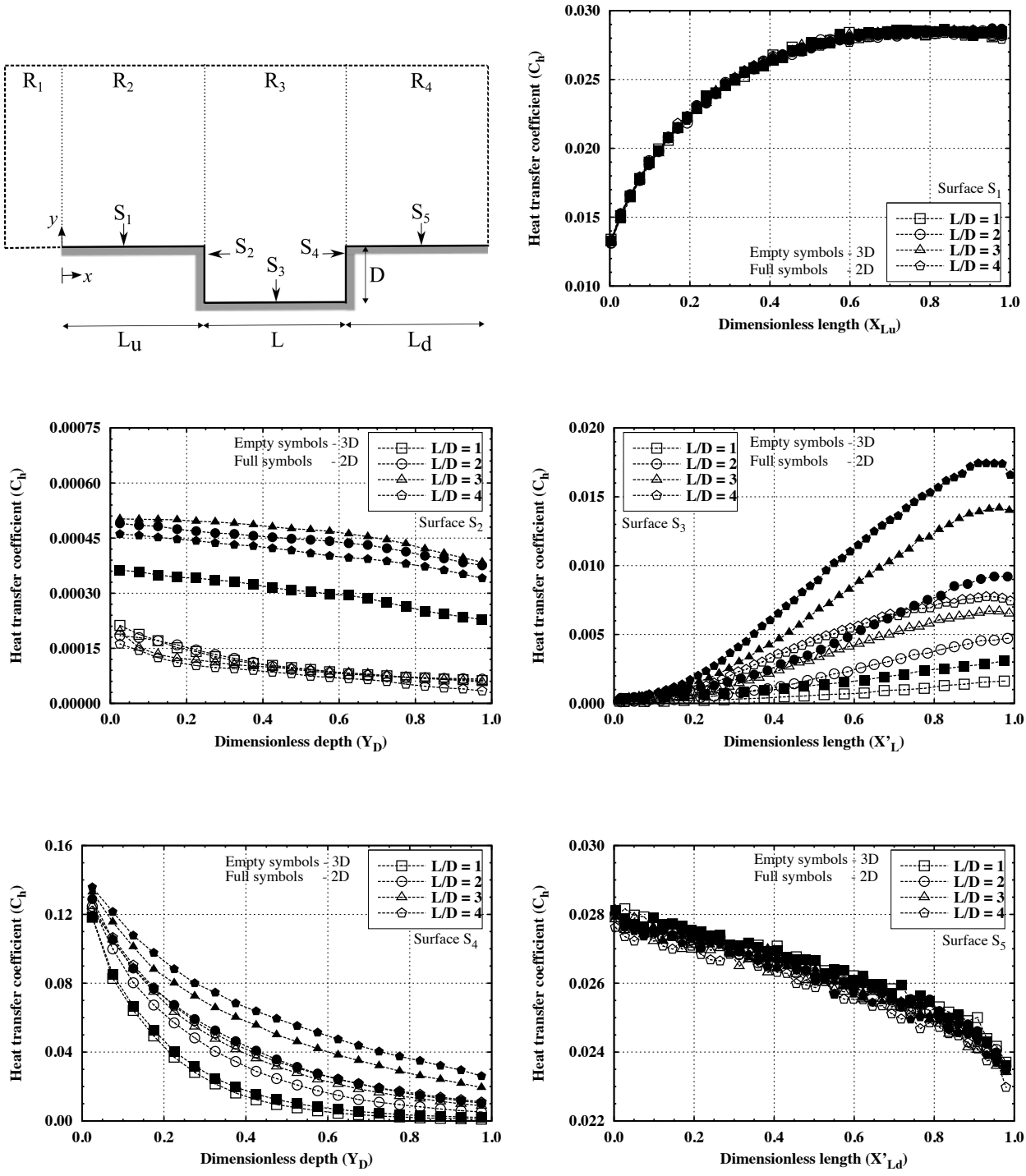

Figure 5. Heat transfer coefficient (C_h) predictions for different cavity L/D ratios.

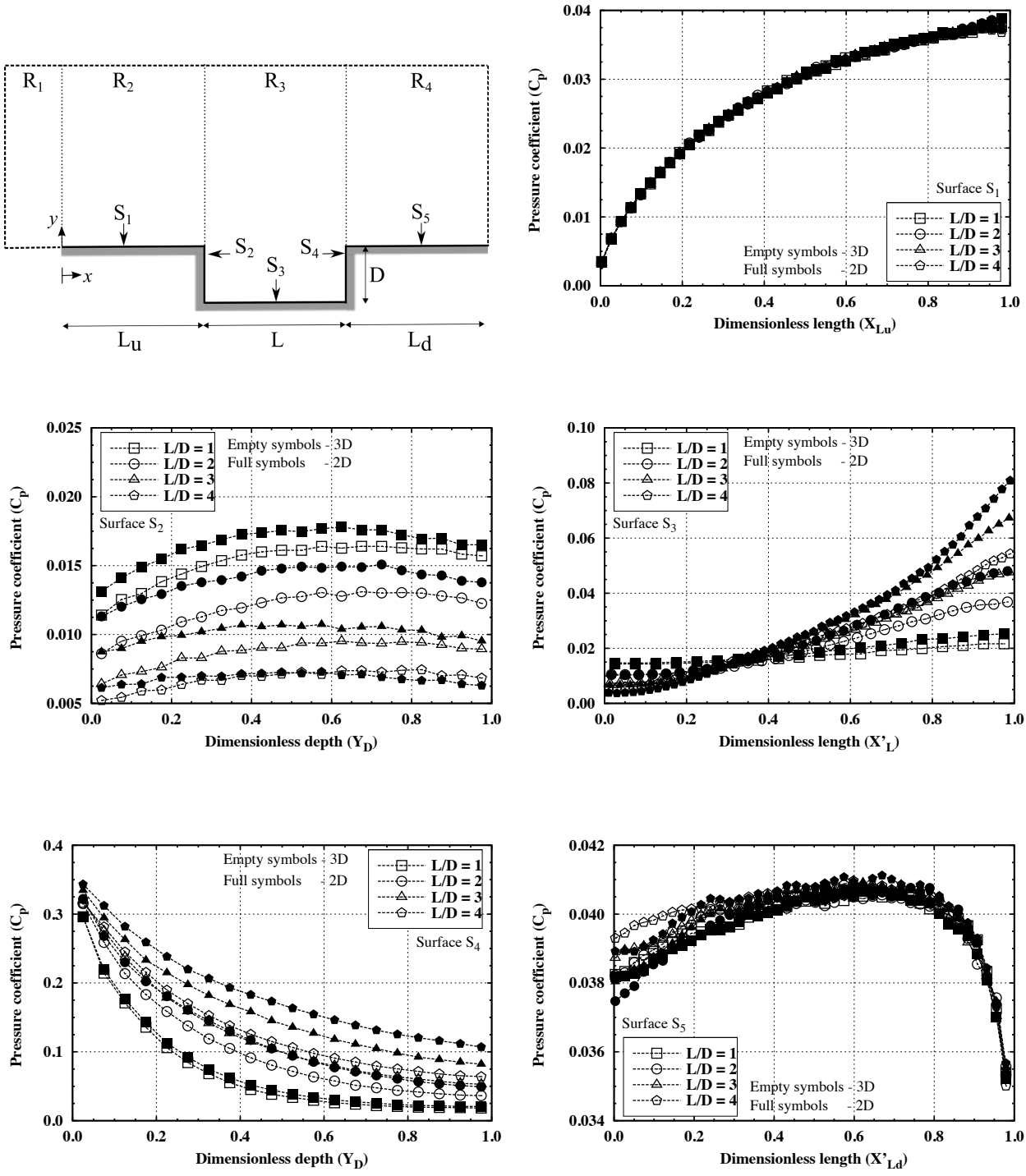

Figure 6. Pressure coefficient (C_p) predictions for different cavity L/D ratios.

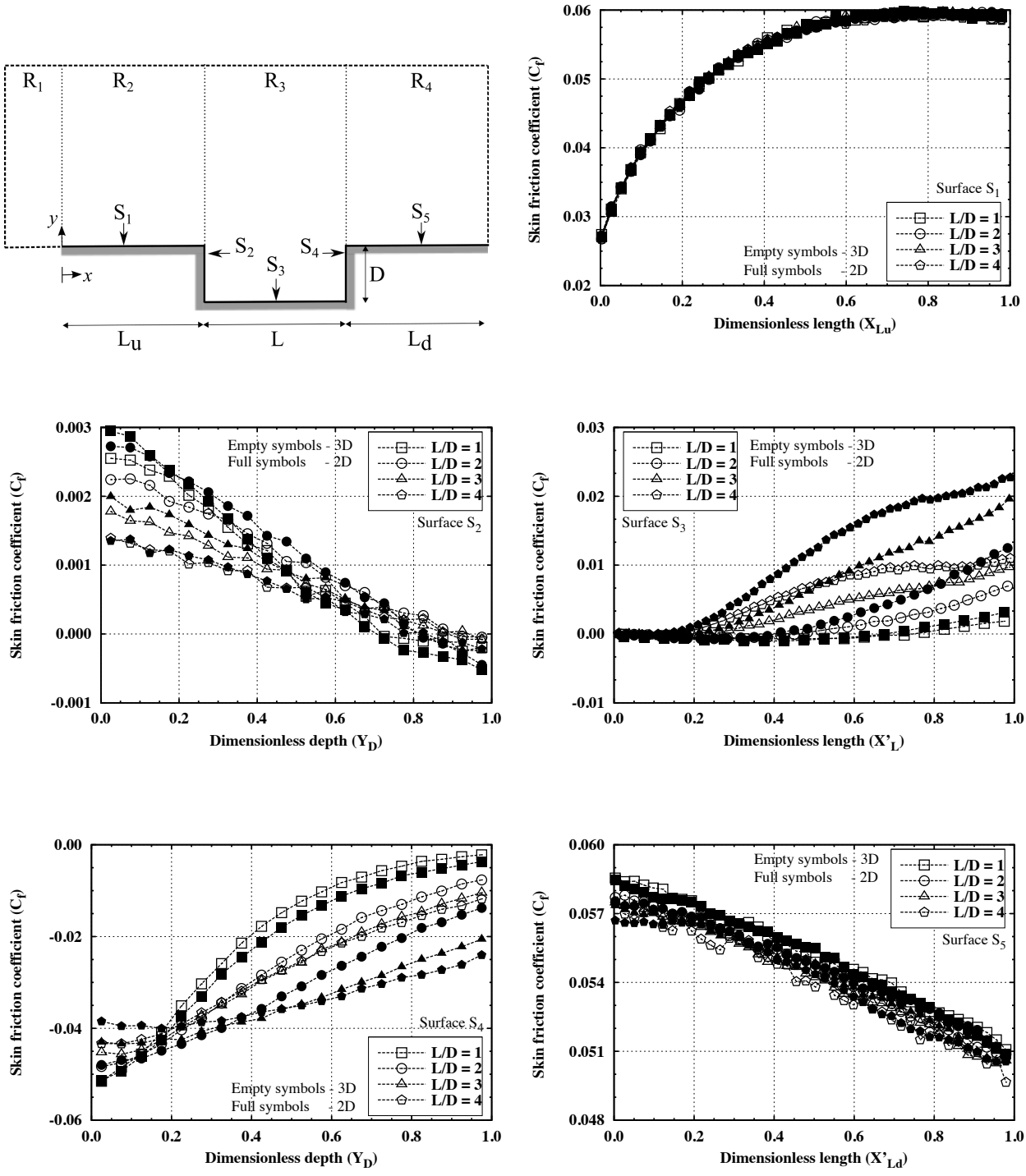

Figure 7. Skin friction coefficient (C_f) predictions for different cavity L/D ratios.

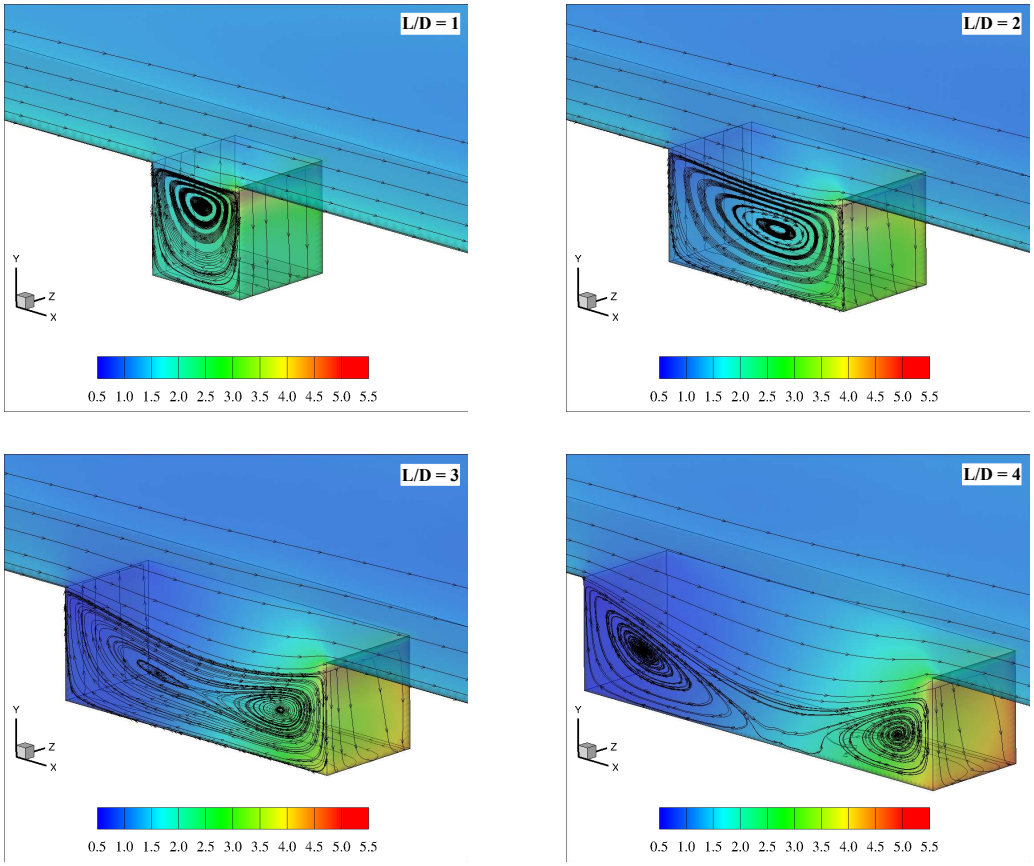

Figure 8. Density ratio (ρ/ρ_∞) contours, with streamline traces inside the cavities (W/2 = 3 mm).

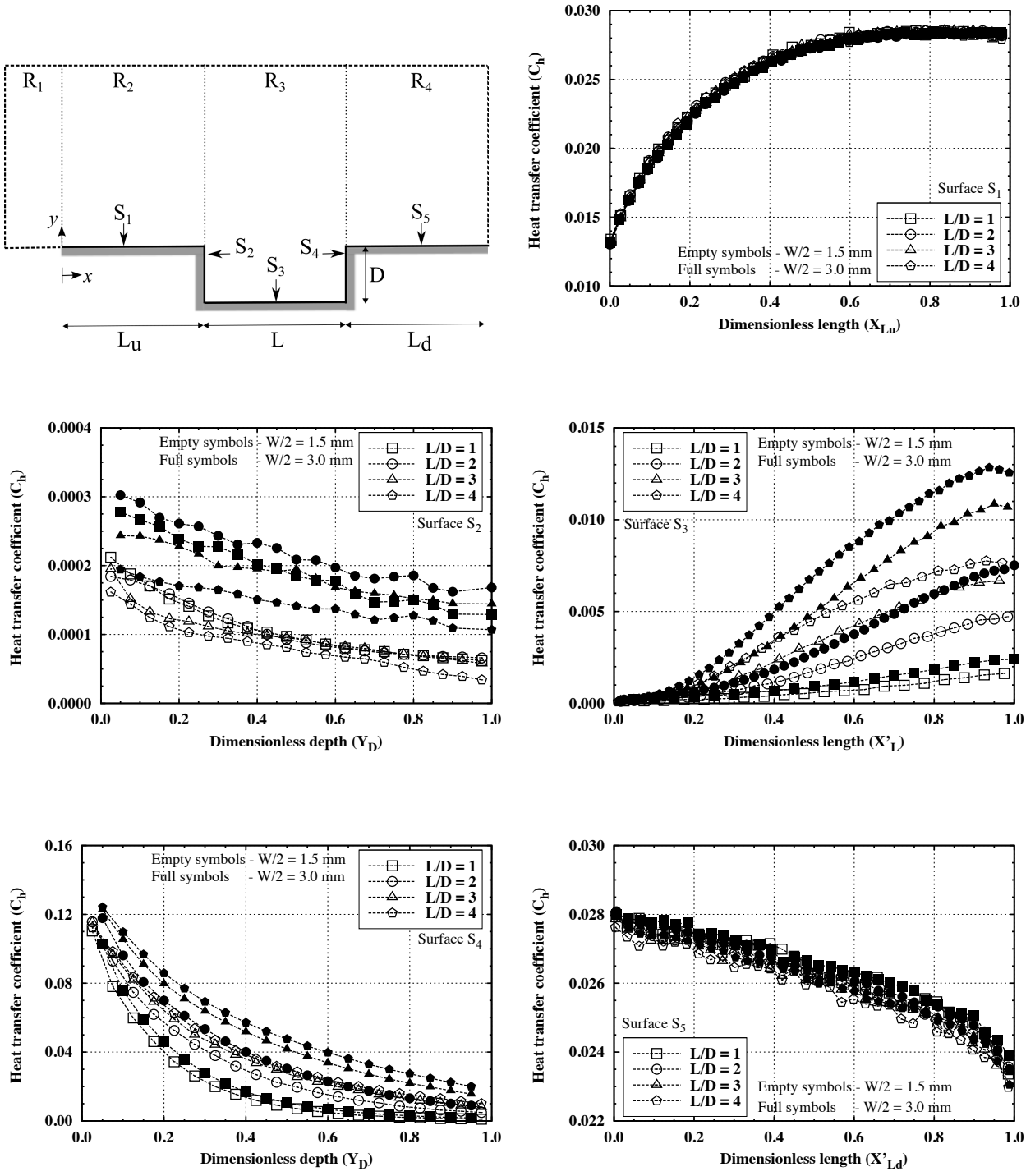

Figure 9. Heat transfer coefficient (C_h) predictions for different cavity widths.

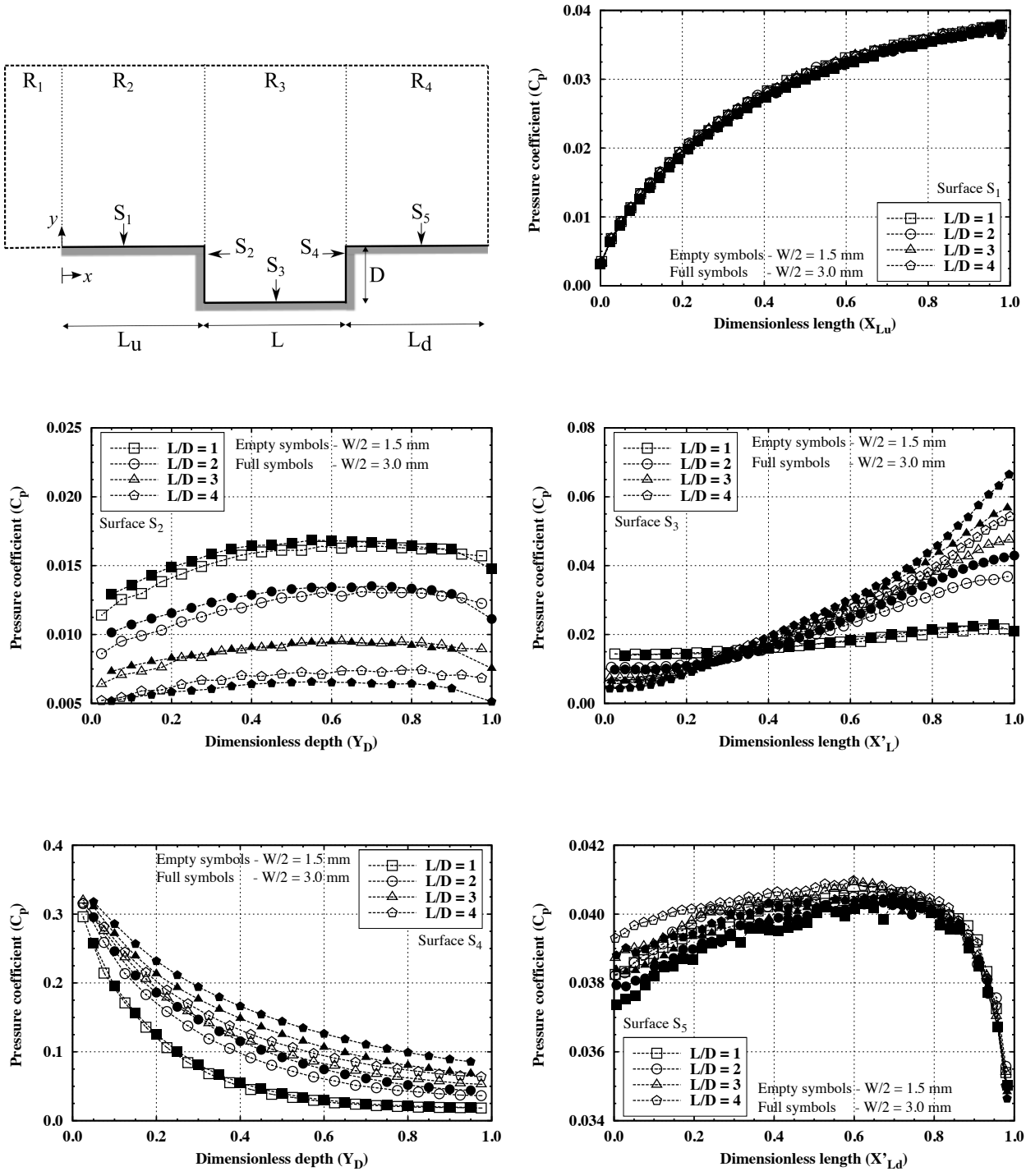

Figure 10. Pressure coefficient (C_p) predictions for different cavity widths.

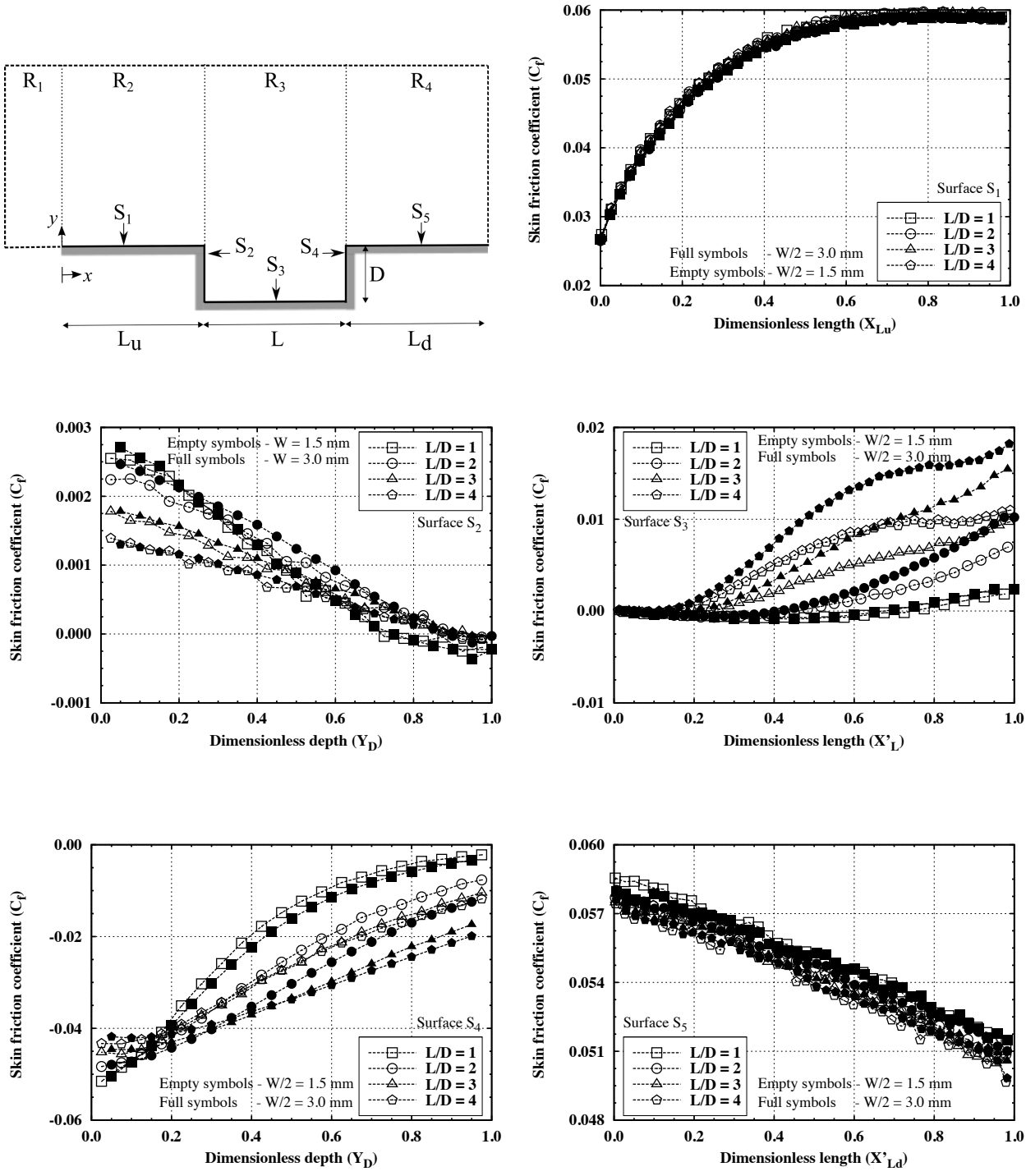

Figure 11. Skin friction coefficient (C_f) for different cavity widths.

VIII. Acknowledgements

The authors would like to acknowledge the financial support provided by Conselho Nacional de Desenvolvimento Científico e Tecnológico under Grant No. 200473/2010-7. Our calculations were performed on the 1100 core High Performance Computing facility of the Faculty of Engineering at the University of Strathclyde.

References

[1]Gallis, M. A., Boyles, K. A., and Lebeau, G. J., "DSMC Simulations in Support of the STS-107 Accident Investigation," *AIP Conference Proceedings*, Vol. 762, Bari, Italy, 2005, pp. 1211–1216.

[2]"Report of Columbia Accident Investigation Board," pp. 49-78, NASA, 2003.

[3]Bird, G. A., "Sophisticated DSMC Short Course," *presented at Direct Simulation Monte Carlo Theory, Methods and Applications conference*, Sandia National Laboratory, Santa Fe, New Mexico, Sept. 2007.

[4]Bird, G. A., Gallis, M. A., Torczynski, J. R., and Rader, D. J., "Accuracy and Efficiency of the Sophisticated direct simulation Monte Carlo Algorithm for Simulating Noncontinuum Gas Flows," *Physics of Fluids*, Vol. 21, 2009.

[5]Candler, G. V., Dimitri, M. J., and Trevino, L., "Current Status and Future Prospects for the Numerical Simulation of Hypersonic Flows," *47th AIAA Aerospace Science Meeting Including the New Horizons Forum and Aerospace Exposition*, No. AIAA 2009-153, Orlando, Florida, 2009.

[6]Charwat, A. F., Roos, J. N., Dewey, C. F. J., and Hitz, J. A., "An Investigation of Separated Flows Part I: The Pressure Field," *Journal of Aerospace Sciences*, Vol. 28, No. 6, 1961, pp. 457–470.

[7]Charwat, A. F., Dewey, C. F., Roos, J. N., and Hitz, J. A., "An Investigation of Separated Flows Part II: Flow in the Cavity and Heat Transfer," *Journal of Aerospace Sciences*, Vol. 28, No. 7, 1961, pp. 513–527.

[8]Bertram, M. H. and Wiggs, M. M., "Effect of Surface Distortions on the Heat Transfer to a Wing at Hypersonic Speeds," *AIAA Journal*, Vol. 1, No. 6, 1963, pp. 1313–1319.

[9]Chang, P. K., "The Reattachment of Laminar Cavity Flow with Heat Transfer at Hypersonic Speed," Tech. rep., United States Air Force Office of Scientific Research, 1966.

[10]Arrington, J. P., Bertram, M. H., Cary, A. M. J., and Weinstein, L. M., "Heat Transfer to Wavy Wall in Hypersonic Flow," *AIAA Journal*, Vol. 5, No. 10, 1967, pp. 1760–1767, AIAA Paper No. 67-164.

[11]Nestler, D. E., Saydah, A. R., and Auxer, W. L., "Heat Transfer to Steps and Cavities in Hypersonic Turbulent Flow," *AIAA Journal*, Vol. 7, No. 7, 1968, pp. 1368–1370.

[12]Charwat, A. F., "Separation of a Supersonic Accelerated Flow over Notches," *AIAA Journal*, Vol. 9, No. 8, 1971, pp. 1656–1657.

[13]Nestler, D. E., "An Experimental Study of Hypersonic Cavity Flow," *Journal of Spacecraft and Rockets*, Vol. 19, No. 3, 1982, pp. 195–196.

[14]Charbonnier, J. M. and Boerrigter, H. L., "Contribution to the Study of Gap Induced Boundary Layer Transition in Hypersonic Flow," *AIAA Journal*, , No. AIAA Paper 93-5111, 1993, 5th International Aerospace Planes and Hypersonic Technologies Conference, Munich, Germany.

[15]Tracy, M. B. and Plentovich, "Characterization of Cavity Flow Fields Using Pressure Data Obtained in the Langley 0.3-Meter Transonic Cryogenic Tunnel," Tech. Rep. NASA 4436, 1993.

[16]Morgenstern, A. J. and Chokani, N., "Hypersonic Flow Past Open Cavities," *AIAA Journal*, Vol. 32, No. 12, 1994, pp. 2387–2393.

[17]Hinderks, M., Radespiel, R., and Gulhan, A., "Simulation of Hypersonic Gap Flow with Consideration of Fluid Structure Interaction," *34th AIAA Fluid Dynamics Conference and Exhibit*, No. AIAA 2004-2238, July, Portland, Oregon 2004, pp. 1–22.

[18]Everhart, J. L., Alter, S. J., Merski, N. R., and Wood, W. A., "Pressure Gradient Effects on Hypersonic Cavity Flow Heating," *44th Aerospace Sciences Meeting and Exhibit*, AIAA Paper No. 2006-185, 2006.

[19]Horvath, T. J., Berry, S. A., Merski, N. R., and Berger, K. T., "Shuttle Damage/Repair from the Perspective of Hypersonic Boundary Layer Transition - Experimental Results," *9th AIAA/ASME Joint Thermophysics and Heat Transfer Conference*, No. AIAA-2006-2919, San Francisco, California, 2006.

[20]Creighton, S. and Hillier, R., "Experimental and Computational Study of Unsteady Hypersonic Cavity Flows," *The Aeronautical Journal*, Vol. 111, No. 1125, 2007, pp. 673–688.

[21]Palharini, R. C. and Santos, W. F. N., "Length-to-Depth Ratio Effects on Flowfield Structure of Low-Density Hypersonic Cavity Flow," No. AIAA-20113130, 42nd AIAA Thermophysics Conference, Jun 2011.

[22]Lofthhouse, A. M., Boyd, I. D., and Wright, J. M., "Effects of Continuum Breakdown on Hypersonic Aerothermodynamics," *Physics of Fluids*, Vol. 19, No. 2, 2007, pp. 1–12.

[23]Lofthhouse, A. M., Scalabrin, L. C., and Boyd, I. D., "Velocity Slip and Temperature Jump in Hypersonic Aerodynamics," *Journal of Thermophysics and Heat Transfer*, Vol. 22, No. 1, 2007, pp. 38–49.

[24]Bird, G. A., *Molecular Gas Dynamics and the Direct Simulation of Gas Flows*, Oxford University Press, Oxford, UK, 1994.

[25]Scanlon, T. J., Roohi, E., White, C., Darband, M., and Reese, J. M., "An Open-Source, Parallel, DSMC Code for Rarefied Gas Flows in Arbitrary Geometries," *Computers and Fluids*, Vol. 39, 2010, pp. 2078–2089.

[26]OpenFOAM, "http://www.openfoam.org/," 2013.

[27]Wagner, W., "A convergence proof for Bird's direct simulation Monte Carlo method for the Boltzmann equation," *Journal of Statistical Physics*, Vol. 66, No. 3-4, 1992, pp. 1011–1044.

[28]Borgnakke, C. and Larsen, P. S., "Statistical Collision Model for Monte Carlo Simulation of Polyatomic Gas Mixture," *Journal of Computational Physics*, Vol. 18, No. 4, 1975, pp. 405–420.

[29]Bird, G. A., "Perception of Numerical Method in Rarefied Gas Dynamics," Vol. 118, Pasadena, CA, 1988, pp. 211–226.

[30]Alexander, F. J., Garcia, A. L., and Alder, B. J., "Cell Size Dependence of Transport Coefficient in Stochastic Particle Algorithms," *Physics of Fluids*, Vol. 10, No. 6, 1998, pp. 1540–1542.

[31]Garcia, A. L. and Wagner, W., "Time Step Truncation Error in Direct Simulation Monte Carlo," *Physics of Fluids*, Vol. 12, 2000, pp. 2621–2633.

[32]Hadjiconstantinou, N. G., "Analysis of Discretization in the Direct Simulation Monte Carlo," *Physics of Fluids*, Vol. 12, No. 10, 2000, pp. 2634–2638.

[33]Anon., "U.S. Standard Atmosphere," *National Oceanic and Atmospheric Administration, NASA, and U.S. Air Force*, Oct. 1976.